SPACE-BORNE SYNTHETIC APERTURE RADAR OF INTERTIDAL FLAT SURFACES AS A BASIS FOR PREDICTING BENTHIC MACROFAUNA DISTRIBUTION

Daphne van der Wal, Peter M.J. Herman and Tom Ysebaert

Netherlands Institute of Ecology (NIOO-KNAW), P.O. Box 140, 4400-AC Yerseke, The Netherlands; d.vanderwal(at)nioo.knaw.nl

ABSTRACT

High resolution, synoptic information on sediment characteristics of tidal flats is required for habitat mapping, and for assessing the distribution of benthic macrofauna. This study aims to derive information on surface characteristics of tidal flats from space-borne Synthetic Aperture Radar (SAR). Estimates of the backscatter coefficient were extracted from ERS-1 SAR and ERS-2 SAR PRI imagery of two tidal flats in the Westerschelde. They were related to field measurements of surface roughness, moisture conditions, sediment characteristics (median grain-size and silt content) and densities of benthic macrofauna. As predicted by the IEM backscattering model, a significant positive relationship was found between surface roughness and the backscatter coefficient: rougher surfaces were associated with higher backscatter values. In addition, median grain-size was positively correlated with backscatter, and silt content was negatively correlated with backscatter. Surface roughness was related to sediment characteristics: sandy sediment was found to be rougher than finer sediment, because surface ripples were more pronounced in the former. Significant relationships were also found between the sediment characteristics and macrofauna density. Relationships between sediment characteristics and backscatter were generally consistent in time. This demonstrates the potential of SAR for habitat mapping.

Keywords: SAR, sediment grain-size, surface roughness, macrozoobenthos

INTRODUCTION

Tidal flats have particular significance for ecosystems of estuaries, as they accommodate a large and diverse biological community. This includes benthic fauna, which play an important role in estuarine food webs, as they are the food supply for wintering and migratory birds. Information on macrobenthos distribution is required to assist in the implementation of coastal management plans and ecological impact assessments, as well as for fisheries. Mapping and monitoring benthic fauna distribution from in situ measurements is, however, severely hampered by the high costs involved in sampling, resulting in very limited numbers of sample points. Many studies have gained insight into the physical factors that determine the geographical distribution of benthic macrofauna on tidal flats. On an estuary-wide scale, such patterns are related to the salinity gradient, and to variations in bathymetry, hydrodynamics and sediment characteristics (1,2,3). On the scale of a tidal flat, sediment grain-size is a key parameter (4). In addition, surface roughness is identified as an important parameter, both for its association with sediment dynamics and the burial depth of infauna, and for its association with hydrodynamics (4). Although the exact nature of the dependence of macrofauna on these environmental conditions is still open to debate (1,5), the information on environmental variables can be used successfully for habitat mapping and prediction of the occurrence of benthic macrofauna (2,3). This requires high resolution, synoptic information on environmental variables. In particular, there is a lack of geographically extensive and detailed information on sediment and roughness characteristics.

Remote sensing is suited for synoptically mapping and monitoring surface characteristics of intertidal flats. Optical remote sensing has been used to characterise the sediment distribution of tidal flats (e.g., 6,7,8,9), but with mixed success. Microwave satellite remote sensing has great potential for mapping and monitoring, as imagery from clouded areas can be used, making radar remote

sensing reliable for planning matching ground truthing. So far, Synthetic Aperture Radar (SAR) has not been used for mapping sediment grain-size. However, numerous studies, especially in the field of agriculture, have demonstrated the dependence of radar backscatter on surface roughness and the dielectric properties of the surface (e.g., 10,11,12). In intertidal areas, radar remote sensing has been used for coastline detection, and for the extraction of bathymetry (e.g., 13,14) and surface roughness (15). The use of SAR for habitat mapping of intertidal flats has received little attention.

The objective of this study is to extract information on the physical characteristics of tidal flats from satellite radar imagery (i.e., ERS SAR), in particular surface roughness and sediment characteristics. In a next stage, this information can then be used for mapping and predicting macrobenthos distribution. Data in support of the information derived from SAR imagery were obtained from field campaigns in 1995/1996 and further ground-truthing in 2003. The focus is on tidal flats of the Westerschelde in the south-western part of the Netherlands.

STUDY AREA

The Westerschelde is a well-mixed macrotidal coastal plain estuary in the south-west of the Netherlands (Figure 1). The estuary is tide-dominated, and experiences a semi-diurnal tide; the mean tidal range increases from 3.8 m near the mouth of the estuary to 5.0 m near the Dutch-Belgian border. Salinity ranges from a marine zone (salinity >18) between the mouth of the estuary and Hansweert (close to the Molenplaat), to a brackish zone (salinity 5-18) reaching beyond the Belgian border. The estuary is a nutrient-rich, heterotrophic system. It is characterized by a complex network of flood and ebb channels surrounding tidal flats. The tidal flats are composed of muddy to sandy sediment, and are generally not vegetated. The study focuses on two mid-channel flats in the Westerschelde: the Molenplaat and the Plaat van Everingen.
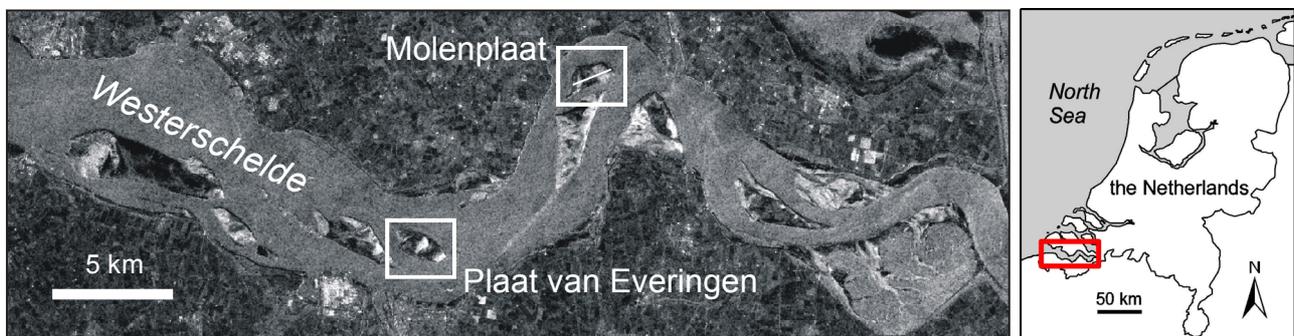

Figure 1: Selected tidal flats in the Westerschelde, The Netherlands. The location of the transect on the Molenplaat is also shown. Detail of the Westerschelde is obtained from an ERS-2 SAR image from 7 April 2003 (image © ESA, 2003).

METHODS

(Pre-)processing of satellite imagery

Images were obtained from the global environmental monitoring satellite ERS-1 and its successor ERS-2 (European Remote Sensing Satellite) of the European Space Agency. The satellites have a Synthetic Radar Aperture (SAR) instrument aboard, an active radar operating at a wave-length of 5.66 cm and a 5.3 GHz frequency (C band), with a VV polarization (vertical transmit, vertical receive). The incidence angle α is 23° at mid-swath, and ranges from 19.5° at near-range to 26.5° at far-range. For this study, I-PAF and UK-PAF precision images (PRI) were used, which are multi-look (noise-reduced), ground range, system-corrected digital images. The ERS SAR PRI data were calibrated following Laur et al. (16). Brightness values β^0 were converted to values of the backscattering coefficient σ^0 using image processing software to allow between-image comparisons. Differences in incidence angle occurring across a swath were included in this conversion. No correction was applied for topographic effects: a flat terrain was assumed for all tidal flats. This was justified,

as slopes were generally below 1°. An average value of the backscatter coefficient was calculated for every pixel in each image, using a moving window of 9x9 pixels (corresponding to ca 117 by 117 m in the field) in order to achieve a radiometric resolution of ±1 dB at mid-swath with approximately 95% confidence (16). The images were rectified and transformed to the Dutch National Grid (a stereographic projection on the Bessel spheroid) using the exact location of over 20 well-distributed bridges and dikes as ground control points, applying a cubic convolution interpolation technique, while retaining the pixel size of 12.5 by 12.5 m. The root-mean-square (RMS) transformation error was about 30 m. In addition to the images with 9x9 moving window pixel averages of the backscatter coefficient that were used for further analysis, speckle filtered images were produced for visualisation only. A three-pass Lee-Sigma speckle filter (17) was applied, using a window size of 3x3, 5x5 and 7x7 pixels, successively. For each pass, the coefficient of variation was calculated and applied, with a multiplier of variation of 0.5, 1 and 2, respectively. Finally, all backscatter coefficients were expressed in decibels.

Table 1 gives the specifications of the selected radar images. The images were selected such that they matched previous field campaigns in 1995/1996, as well as a field campaign in 2003. Specifications of the conditions during overpass of the satellites are given in Table 2.

Table 1: Specifications of the selected ESA ERS SAR imagery, with the average local incidence angle for the selected tidal flats. Dates of matching field campaigns are also given.

Satellite	Date and time (UTC)	Pass type	Orbit	Track	Frame	Local incidence angle (°)	Matching field work
ERS-1	2 Jul 1995 10:41	Desc	20723	194	2565	21.9 (Molenplaat)	30 Jun 1995 (Molenplaat)
ERS-2	27 Sep 1995 10:38	Desc	02281	423	2565	25.2 (Molenplaat)	30 Sep 1995 (Molenplaat)
ERS-2	25 Dec 1995 10:41	Desc	03555	194	2565	21.8 (Molenplaat)	20 Dec 1995 (Molenplaat)
ERS-2	16 Oct 1996 10:38	Desc	07792	423	2565	25.6 (Everingen) 25.2 (Molenplaat)	15 Oct 1996 (Everingen) 16 Oct 1996 (Molenplaat)
ERS-2	7 Apr 2003 10:40	Desc	41631	194	2565	21.9 (Molenplaat)	24 Mar 2003, 7-8 Apr 2003 (Molenplaat)

Table 2: Conditions during acquisition of ERS SAR imagery. Daily averages of air temperature, cloud cover, wind speed and direction and total daily precipitation from station Vlissingen were obtained from the Royal Netherlands Meteorological Institute. 10 Minute averages of wave height (station Euro platform) and water level and tidal stage (station Hansweert) during overpass were obtained from Rijkswaterstaat. Wave height and water level are relative to the Dutch ordnance datum NAP, which is about mean sea level. All stations are within the coverage of the images.

Date	Air temp. (° C)	Precipitation (mm)	Cloud cover	Wind speed (m/s)	Wind direction (°)	Wave height (m NAP)	Water level (m NAP)
2 Jul 1995	18.1	2.6	7/8	3.6	58 (ENE)	0.99	-2.11, outgoing
27 Sep 1995	13.4	12.4	7/8	8.7	281(W)	2.03	-1.43, incoming
25 Dec 1995	2.6	< 0.05	4/8	6.7	271 (W)	1.10	-2.34, low water
16 Oct 1996	11.7	0.0	4/8	5.1	211 (SSW)	0.88	-2.14, incoming
7 Apr 2003	3.8	0.0	1/8	5.0	58 (ENE)	-	-2.05, outgoing

Field campaigns 1995/1996

In situ data were obtained from field campaigns for the BEON MICRO-MACRO and ECOFLAT projects in 1995/1996 (4,18). These data were collected on the two tidal flats during low tide (Tables 1

and 2). Sediment characteristics and benthic macrofauna were sampled in a rectangular grid, with a spacing of 150 m (1995 data set) to 300 m (1996 data set) between the sample points. A Global Positioning System (GPS), with an accuracy of about 5 m was used for positioning. Samples were taken of the upper 1 cm of the sediment, and the median grain-size and the amount of silt (i.e. percentage of particles smaller than 63 μm) of these samples were determined using a Malvern particle sizer. In addition, samples with a diameter of 11 cm were taken of the upper 30 cm of the sediment. This material was sieved over a 1 mm sieve, and the residue was fixed in buffered formaldehyde. All animals in each core were identified under the microscope, and macrofauna density and biomass per species were determined. Detailed bathymetry from selected tidal flats for 1996 (grid with 20 by 20 m cells) and 2001 (grid with 5 by 5 m cells) was obtained from Rijkswaterstaat, from echo sounding and laser altimetry, respectively. Information on sediment, macrofauna and bathymetry of sample points was then joined to estimates of backscatter coefficients (derived from matching ERS SAR imagery) in a Geographical Information System (GIS). Sample points located at heights below -1.50 m NAP (Dutch Ordnance Datum, which is about mean sea level) were excluded from analysis; these were samples located at the edge of the tidal flats that may have been covered by water.

Field campaign 2003

Ground truthing also took place on the Molenplaat during low tide in March and April 2003 (Table 1). Samples were collected along a transect (Figure 1) that was orientated west-east in order to span the environmental conditions present (i.e., sand and mud). Sampling sites were located using a GPS with 4 m accuracy. The percentage of surface water (i.e., pond water) was estimated in 30 m wide areas along the transect. At selected sampling sites along the transect, 60 m apart, 20 cm^3 of sediment was taken in duplo from the upper 3 cm of the sediment. One set of samples was weighed, oven-dried and reweighed, and volumetric moisture contents were determined. The second set of samples was weighed, freeze-dried and reweighed, and volumetric moisture contents of these samples were determined for comparison with the first set. The second set of samples was further used to determine the sediment grain-size distribution, including silt content and median grain-size, using a Malvern particle sizer. Grain-size parameters from the 2003 sediment samples could not be compared with the 1995/1996 sediment data.

Surface roughness was measured in the field. The orientation of surface ripples, as well as the horizontal distance between crests (ripple length), and the height between the crests and troughs of the ripples (ripple height) were measured. At each sampling point, photographs of the surface were taken. Several sampling points were revisited and photographed each day to confirm that ripple orientation and geometry were persistent on a time-scale of days. Surface roughness was also recorded using a white grid board of 0.85 m length and 0.50 m height placed level and perpendicular to the ground. In case of random roughness, a random orientation of the grid board was chosen, with two replicates. In case of orientated ripples, the grid board was placed perpendicular to the ripple direction, with two replicates, and once along the ripple direction. In addition, the grid board was placed perpendicular to the look direction of the sensor, with two replicates. Digital photographs of the grid board were georeferenced and geocorrected using image processing software. An unsupervised classification of the image with 9 clusters was made, which were merged to enable distinction of grid board and sediment, and converted to polygons. Micro-topographic profiles were then extracted to obtain values of relative height every 0.25 cm along the board. A number of statistical descriptors of surface roughness were derived from these profiles. First, the root-mean-square of the heights (RMSz), from which slope bias was removed by subtracting a linear regression line from the profile, was calculated. Then, a correlation function $\rho(\xi)$, a measure for correlation between the height at a certain point and the height at a point ξ distant from that point was determined from the detrended profile, and a correlation length L, for which holds $\rho(L) = e^{-1}$ was calculated following Ulaby et al. (10). The correlation function was found to be exponential.

The field data were joined in a GIS to the estimated backscatter coefficients derived from the ERS-2 SAR image of 7 April 2003. Regression analysis was undertaken on the data to test the hypothesis that in the linear model y = α + $\beta \cdot$x + ε, the parameter β differs from zero, and that there is,

therefore, a linear relation between x and y, explaining at least part of the variation in y. A significance level of 0.05 was applied.

Modelling

Many studies have been undertaken in radar remote sensing research to understand the (surface) backscattering response from natural surfaces and to retrieve surface conditions, such as moisture content and roughness. In particular, analytical electromagnetic backscattering models have been developed for different roughness conditions (10,19). An example is the Integral Equation Model (IEM) developed by Fung (19,20). This model has a broad validation domain. In this study, an approximate solution of the IEM was applied (11), to test the sensitivity of the radar backscatter to roughness, moisture and sediment characteristics, and to assist in interpreting the SAR images.

RESULTS

Sensitivity analysis

The IEM predicts that, for a given radar configuration (i.e., radar wavelength, incidence angle and polarization), the backscatter depends on the dielectric properties of the sediment ε, the vertical roughness parameter RMSz, the horizontal roughness parameter correlation length L and the correlation function.

The dielectric properties of the sediment depend mostly on moisture conditions. During the field campaign in March/April 2003, volumetric moisture constant Mv ranged from 0.2 to 0.7 g cm^{-3}, with Mv generally above 0.45 g cm^{-3}. Using the equation formulated by Topp et al. (cited in 11), which was found to be valid for a wide range of conditions and soil types, this results in a dielectric constant $10 < \varepsilon < 60$, with ε generally above 25. The IEM predicts that ERS SAR backscatter is not very sensitive to variations in such high values for the dielectric constant (Figure 2a). The dielectric constant also depends on the grain-size distribution of the sediment. For a particular volumetric soil moisture, the real component of the dielectric constant is greater for sand (due to the greater availability of free water) than for silt, resulting in a greater backscatter coefficient. This effect, calculated using an empirical relationship by Hallikainen et al. (21) can, however, be neglected. The effect of salinity of the soil water on the dielectric constant can also be neglected when $\varepsilon > 10$ (10). Thus, variations in dielectric constant will only affect radar backscatter on tidal flats to a minor degree. However, if a (thin) layer of water is present on the surface, a specular reflection (no backscatter) is expected (during conditions of low wind speed).
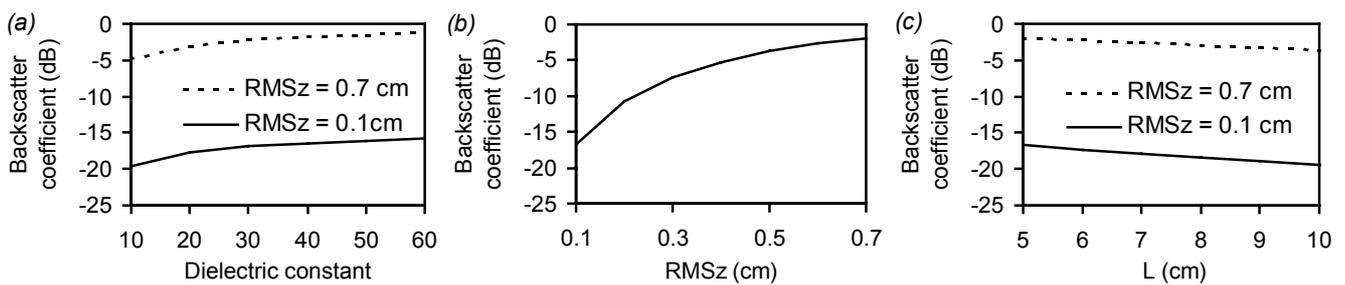

Figure 2: Simulated response of the ERS SAR backscatter coefficient at mid-swath (α = 23°) to (a) the dielectric constant ε, for a smooth (RMSz = 0.1 cm) and medium rough (RMSz = 0.7 cm) surface (L = 5 cm), (b) surface roughness RMSz (L = 5 cm, ε = 35) and (c) correlation length L, for a smooth (RMSz = 0.1cm) and medium rough (RMSz = 0.7 cm) surface (ε = 35), as predicted by the IEM (11,20).

Roughness on tidal flats is mainly determined by the presence of surface ripples. Ripples were regarded as random surface elements in this study. Under the ERS SAR configuration, the Rayleigh criterion implies that a surface with random roughness may be considered smooth when RMSz < 0.77 cm. Peake and Oliver proposed a more subtle classification, with smooth surfaces for RMSz < 0.25 cm, and rough surfaces for RMSz > 1.54 cm (22). On the Molenplaat, roughness (measured perpendicular to the ripple direction) was smooth to intermediate, with 0.1 < RMSz < 0.7 cm. Dif-

ferences between replicates were of the order of 0.1 cm for surfaces with high values of RMSz, and of the order of 0.01 cm for surfaces with low values of RMSz. Figure 2b shows that the IEM predicts large differences in backscatter for the range in roughness values found.

The correlation length L measured on Molenplaat in March/April 2003 was generally L < 10 cm. For low values of L, the IEM is not valid. For 5 < L < 10 cm, The IEM predicts a relatively small range of backscatter values (Figure 2c). Field measurements show that values for correlation length varied considerably between replicates. Given this variability and given the short length of the grid board, measured values for L have to be considered with caution (23). Therefore, in the remainder of this paper, a mean value of L = 5 cm is used.

Radar backscatter and measurements from the 2003 field campaign

Figure 3 shows a number of variables measured along a transect on the Molenplaat during over-pass of ERS-2 SAR on 7 April 2003. A variety of bedforms was present at a range of spatial scales, but small ripples formed by ebb-currents dominated. In general, roughness was least in the central part of the tidal flat. Here, ripples were aligned in a north-south direction, whereas in the outer west and east, ripple orientation was either NE-SW or NW-SE. In the east, surface ripples were superimposed on 10 cm high mega-ripples, with a 15 m crest to crest distance, aligned in a NNW-SSE direction. These megaripples were regarded as meso-topography, not surface rough-ness. The roughness parameters showed the same trends along the profile (Figures 3b and 3c): RMSz correlated positively with both ripple length (R^2 = 0.53) and ripple height (R^2 = 0.68).

The estimates of the backscatter coefficient (Figure 3a) also correlated with the surface roughness parameters (Figures 3b and 3c; Table 3). Backscatter along the transect was positively correlated with RMSz measured perpendicular to the ripple direction (R^2 = 0.56), and to a lesser extent with RMSz measured perpendicular to the look direction of the sensor (R^2 = 0.41), ripple length (R^2 = 0.53) and ripple height (R^2 = 0.45), but all relationships were significant. The dependence of backscatter on roughness is further illustrated in Figure 4a. Although the relationship between RMSz and backscatter was significant, and the backscatter estimates at the sample locations gen-erally matched the backscatter predicted by the IEM, a degree of scattering of the measurements was apparent.

Table 3: Results of the linear regression analysis of surface characteristics obtained from field measurements or sampling for the Molenplaat, with the backscatter coefficient estimate derived from matching ESA ERS SAR imagery as the dependent variable, giving the coefficient of determi-nation (R^2), probability (p) and number of observations (n).

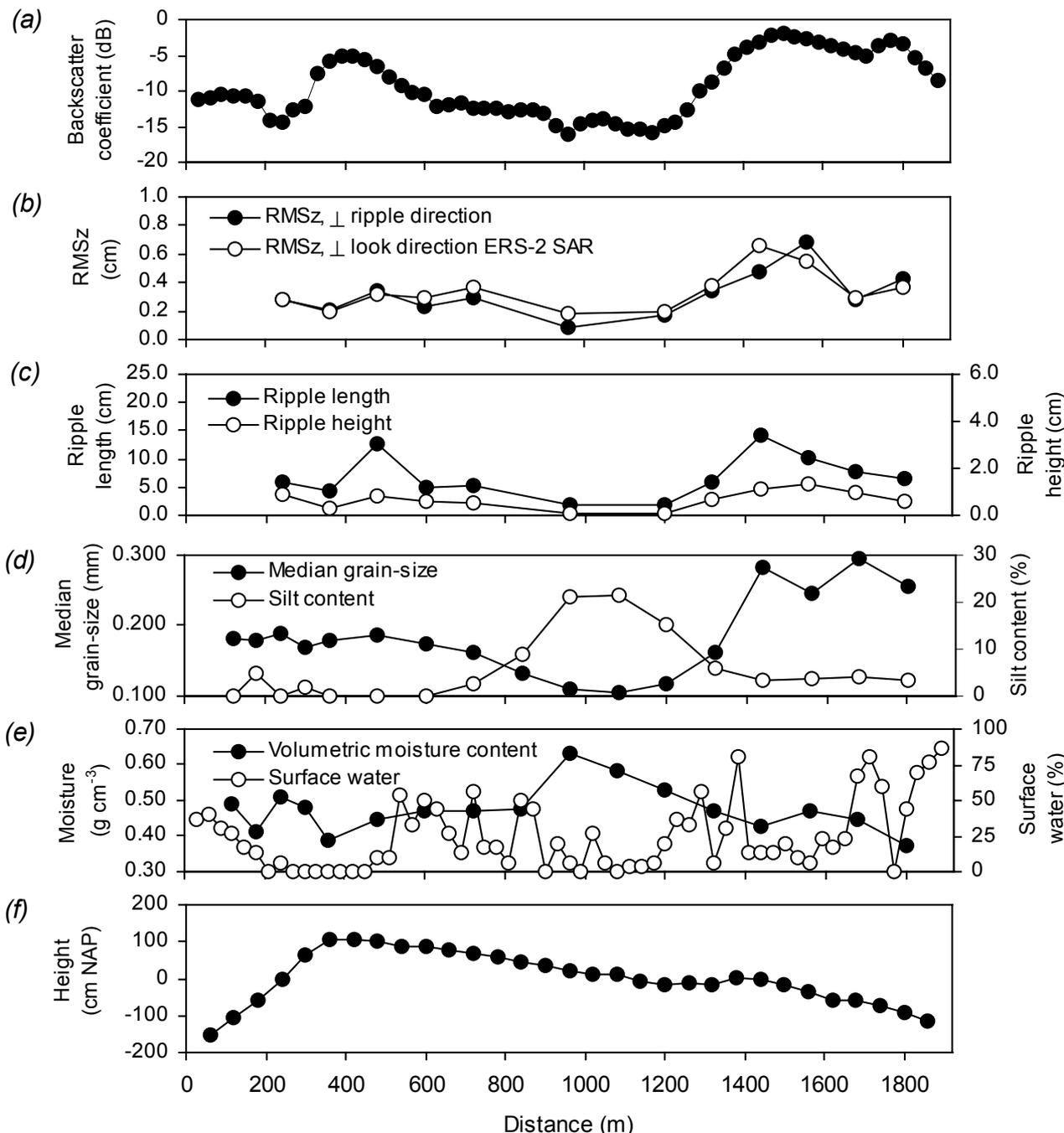| Date	Median grain-size (mm)	Silt content (%)	RMSz (cm)	Moisture content (g cm^{-3})	Water surface (%)	Bathymetry (m NAP)
Jun/Jul 1995	R^2 = 0.45 p = 0.000 n = 88	R^2 = 0.51 p = 0.000 n = 88	-	-	-	R^2 = 0.00 p = 0.859 n = 88
Sep 1995	R^2 = 0.45 p = 0.000 n = 88	R^2 = 0.56 p = 0.000 n = 88	-	-	-	R^2 = 0.23 p = 0.000 n = 88
Dec 1995	R^2 = 0.44 p = 0.000 n = 88	R^2 = 0.46 p = 0.000 n = 88	-	-	-	R^2 = 0.09 p = 0.004 n = 88
Oct 1996	R^2 = 0.60 p = 0.000 n = 22	R^2 = 0.62 p = 0.000 n = 22	-	-	-	R^2 = 0.04 p = 0.381 n = 22
Mar/Apr 2003	R^2 = 0.74 p = 0.000 n = 17	R^2 = 0.28 p = 0.029 n = 17	R^2 = 0.56 p = 0.005 n = 12	R^2 = 0.54 p = 0.001 n = 17	R^2 = 0.03 p = 0.153 n = 63	R^2 = 0.04 p = 0.294 n = 31

Figure 3: (a) ERS-2 SAR backscatter coefficient estimates and (b-f) field measurements of environmental conditions during satellite overpass along a west-east orientated transect, Molenplaat, 7 April 2003.

Silt contents along the transect are given in Figure 3d. Percentages of silt were notably high in the central part of the tidal flat. A significant, but weak correlation ($R^2 = 0.28$) was found between silt content and estimates of the backscatter coefficient (Table 3). High silt contents (Figure 3d) were associated with smooth surfaces (Figures 3b and 3c), but the relationships between silt content and the roughness parameters were generally not significant. Median grain-size had a positive significant correlation with backscatter coefficient estimates ($R^2 = 0.74$, see Figure 4b). Median grain-size was also significantly correlated with the roughness parameters RMSz ($R^2 = 0.46$), ripple length ($R^2 = 0.50$) and ripple height ($R^2 = 0.65$): the finer the sediment, the smoother the surface.

Figure 3e shows the values for moisture and inundation along the transect, measured during satellite overpass. There was a significant negative correlation between backscatter coefficient esti-

mates and measured volumetric moisture (R^2 = 0.54), in contrast to predictions by the IEM that show a positive correlation (Figure 2a). Higher moisture contents were associated with higher silt content (R^2 = 0.57) and finer median grain-size (R^2 = 0.43). The percentage of water ponding on the surface (Figure 3e) was substantial in places. Water ponding in the troughs of small ripples was found along most of the sampled transect during satellite overpass, except for the dry area between ca 200 and 400 m. No apparent relationship was found between backscatter values and the percentage of surface water during overpass nor between backscatter values and elevation (Figure 3f, Table 3).

Figure 4: (a) RMSz values (measured perpendicular to the ripple direction) versus the backscatter coefficient estimates derived from an ESA ERS-2 SAR image, Molenplaat, 7 April 2003. The dotted line shows the backscatter as predicted by the IEM for the measured RMSz (with ε = 35, L = 5 cm and α = 21.9°) (b) median grain-size versus backscatter coefficient estimates, Molenplaat, 7 April 2003. The bold lines show linear regression lines, with the regression equations.

Radar backscatter and measurements from the 1995/1996 field campaigns

The relationships observed between radar backscatter and environmental conditions measured along a transect on the Molenplaat were confirmed by historical sets of field data and matching ERS-1 and ERS-2 SAR imagery.

Figure 5 shows the relationship between median-grain size and radar backscatter on the two selected tidal flats in October 1996: finer median grain-sizes were associated with lower estimates of the backscatter coefficient. Linear relationships were significant (Table 3). Statistics to test the differences between the two regression equations revealed that the slope of the regression lines was not significantly different, but the intercept differed significantly, with the Everingen data having the lowest offset. However, this outcome should be treated with some caution, as small median grain-sizes were absent on the Plaat van Everingen.
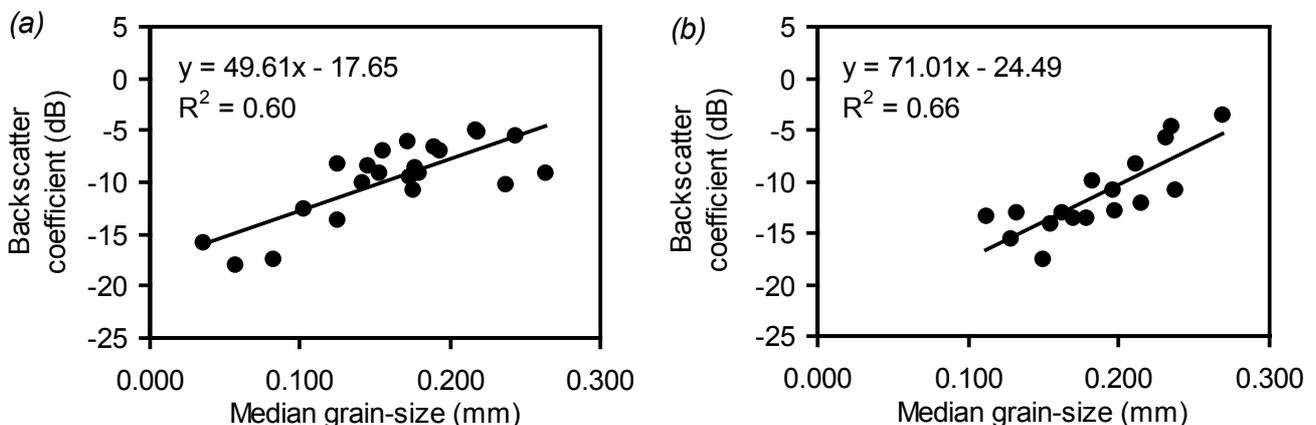

Figure 5: Relationship between sampled median grain-size and backscatter coefficient estimates derived from an ESA ERS-2 SAR image, for (a) the Molenplaat, and (b) Plaat van Everingen, October 1996. The bold lines show linear regression lines, with the regression equations.

The distribution patterns of sediment characteristics and benthic macrofauna were studied in detail on the Molenplaat. Maps of silt content (Figure 6b) and benthic macrofauna densities (Figure 6c) were constructed from field measurements using a Kriging interpolation technique, applying a best fit linear variogram model. In June 1995, silt content and benthic macrofauna were highest in the central part of the tidal flat. The patterns corresponded to those observed on the matching ERS-1 SAR image (Figure 6a).
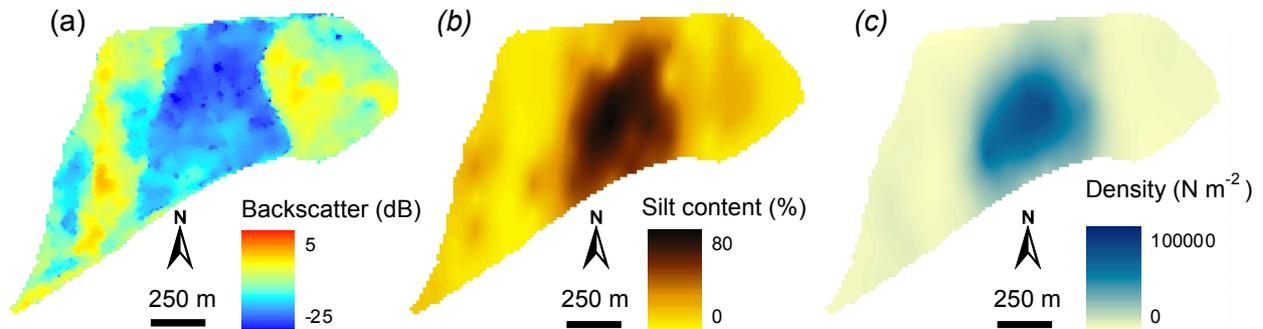

Figure 6: (a) Backscatter derived from a speckle-filtered ESA ERS-1 SAR image, (b) sampled silt content, and (c) sampled total benthic fauna density, Molenplaat, June/July 1995. Outline is the -1.50 m NAP contour line.

Corresponding scatter plots revealed significant relationships between silt content and backscatter (Figure 7a), and between median grain-size and backscatter. Similar relationships were found between silt content and backscatter, and between median grain-size and backscatter, both for September 1995, December 1995 and October 1996. The correlations were all significant (Table 3). Moreover, the slope and intercept of the regression equation found for the Molenplaat in June/July 1995 (Figure 7a) were not significantly different from those for September 1995 and October 1996. Only for December 1995, a significantly higher offset was found, both for silt content and for median grain-size.
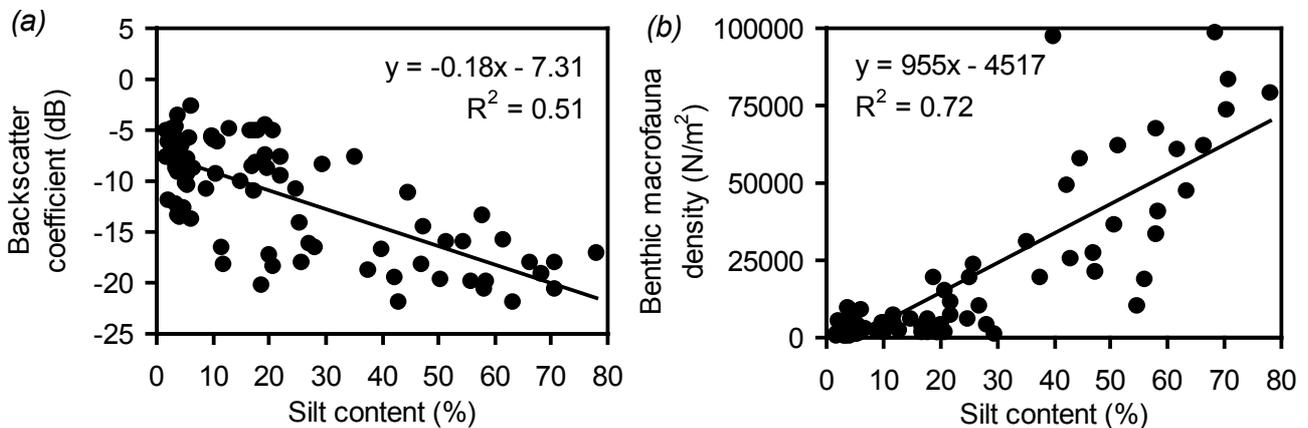

Figure 7: Relationship between (a) sampled silt content and backscatter coefficient estimates derived from an ESA ERS-1 SAR image, and (b) sampled silt content and total density of benthic macrofauna, Molenplaat, June/July 1995. The bold lines show linear regression lines.

Significant positive relationships were also found between silt content and total macrofauna density (for example Figure 7b for June/July 1995) and between median grain-size and macrofauna density. Densities and biomasses of many species showed a significant positive correlation with sediment characteristics, including species with a high abundance, such as the burrowing deposit feeder *Heteromastus filiformus*, the surface deposit feeders *Macoma balthica*, *Pygospio elegans* and *Polydora ligni*, and the omnivore *Nereis succinea*. For a number of other abundant species, including *Nereis diversicolor* and *Arenicola marina*, correlation with silt content and median grain-size was weak or more complex. A select number of species, such as *Bathyporeia pilosa*, only occurred in highly dynamic, sandy places with low silt content.

CONCLUSIONS

This study has demonstrated the potential of radar remote sensing for mapping of surface characteristics of tidal flats.

Ripple structure and sediment grain-size parameters were significantly related to backscatter coefficient estimates derived from ERS SAR imagery. Rougher surfaces, associated with surface ripples, were related to higher backscatter values. Larger median-grain sizes as well as lower silt contents were also associated with higher backscatter values. Surface ripple formation depends on current velocities and direction during inundation and on sediment grain-size. Surface ripples best form in sand and coarse silt, which are relatively easy to transport and erode. In silt and mud, cohesion is generally too large relative to the shear stresses for surface ripples to form.

Large-scale patterns of sediment parameters and macrobenthos densities corresponded to patterns in backscatter on ERS SAR imagery. In addition, the distribution of sediment characteristics was significantly correlated with densities of benthic macrofauna.

The positive relationships between median grain-size and the backscatter coefficient estimates and the negative relationships between silt content and the backscatter coefficient estimates were significant for all images. In addition, relationships were generally consistent in time (for the dates studied). This demonstrates the relevance of the regression equations for future modelling. Further testing is required to establish the differences in backscatter response between tidal flats.

However, the scatter plots of surface characteristics versus backscatter coefficient estimates (Figures 4, 5 and 7a) showed a considerable amount of scattering, and the coefficients of determination of the regressions (Table 3) were generally low, limiting the predictive power of the regression equations for use in further modelling. In this study, sample averages were used for each location, representing an area of about 117 by 117 m, improving radiometric resolution at the cost of spatial resolution. Geostatistical analysis has demonstrated that averaging values of sediment characteristics over such an area is justified when studying the large-scale distribution patterns of sediment grain-size on these tidal flats. However, other factors may be responsible for the moderate relationship between surface characteristics and backscatter coefficient estimates. These include the variation in roughness parameters and water surfaces on a scale of tens of metres and the potential occurrence of Bragg scattering (10).

The Integral Equation Model (19,20) predicted that the moisture content of the sediment was too high to influence radar backscatter on tidal flats. This study confirmed that soil moisture content played a subordinate role: a spurious negative correlation between moisture content and estimates of the backscatter coefficient was found, as higher soil moisture contents were associated with finer sediments, and hence, smoother surfaces. In contrast, the presence of ponding water was expected to suppress radar backscatter. The presence of surface water is expected to be governed by tidal state and bathymetry, determining the duration of exposure, and also by sediment characteristics. A preference of surface water to stay on poorer drained, finer sediment could have enforced the relationship between sediment characteristics and backscatter. The results from this study did not reveal a (negative) relationship between percentage of surface water and radar backscatter, nor, in general, between bathymetry and backscatter. SAR imagery acquired at a slightly later tidal stage (i.e., ca. three hours after low water, when ponding was found to be minimal, and yet moisture content was still sufficiently high) can be a basis for further research in order to minimise this factor.

The results presented in this paper are encouraging, but the method needs further testing. This will optimize derivation of surface characteristics from SAR imagery, which will subsequently allow modelling and mapping of macrofauna distribution.

REFERENCES

1   Wolff W J, 1983. Estuarine benthos. In : <u>Ecosystems of the World, 26 : Estuaries and Enclosed Seas</u>, edited by B H Ketchum (Elsevier, Amsterdam), 151-180

2   Ysebaert T, P Meire, P M J Herman & H Verbeek, 2002. Macrobenthic species response surfaces along estuarine gradients: prediction by logistic regression. <u>Marine Ecology Progress Series</u>, 225: 79-95

3   Ysebaert T & P M J Herman, 2002. Spatial and temporal variation in benthic macrofauna and relationships with environmental variables in an estuarine, soft sediment environment. <u>Marine Ecology Progress Series</u>, 244: 105-124

4   Herman P M J, J J Middelburg & C H R Heip, 2001. Benthic community structure and sediment processes on an intertidal flat: results from the ECOFLAT project. <u>Continental Shelf Research</u>, 21: 2055-2071

5   Snelgrove P V R & C A Butman, 1994. Animal-sediment relationships revisited: cause versus effect. <u>Oceanography and Marine Biology: an Annual Review</u>, 32: 111-177

6   Bartholdy J & S Folving, 1986. Sediment classification and surface type mapping in the Danish Wadden Sea by remote sensing. <u>Netherlands Journal of Sea Research</u>, 20: 337-345

7   Yates M G, A R Jones, S McGrorty & J D Goss-Custard, 1993. The use of satellite imagery to determine the distribution of intertidal surface sediments of the Wash, England. <u>Estuarine, Coastal and Shelf Science</u> 36: 333-344

8   Kokke, J J M, 1995. <u>Mapping of Sediment Distribution in Intertidal Areas with Optical Remote Sensing</u>. BCRS report 94-15. (BCRS)

9   Rainey, M P, A N Tyler, R G Bryant & D J Gilvear, 2000. The influence of surface and interstitial moisture on the spectral characteristics of intertidal sediments: implications for airborne image acquisition and processing. <u>International Journal of Remote Sensing</u>, 21: 3025-3038

10   Ulaby F T, R K Moore & A K Fung, 1986. <u>Microwave Remote Sensing, Active and Passive, Volume III: From Theory to Applications</u>. (Artech House).

11   Altese E, O Bolognani & M Mancini, 1996. Retrieving soil moisture over bare soil from ERS1 synthetic aperture radar data: sensitivity analysis based on a theoretical surface scattering model and field data. <u>Water Resources Research</u>, 32: 653-661

12   Tansey K J & A C Millington, 2001. Investigating the potential for soil moisture and surface roughness monitoring in drylands using ERS SAR data. <u>International Journal of Remote Sensing</u>, 22: 2129-2149

13   Mason D C & I J Davenport, 1996. Accurate and efficient determination of the shoreline in ERS-1 SAR images. <u>IEEE Transactions on Geoscience and Remote Sensing</u>, 34: 1243-1253

14   Calkoen C J, G H F M Hesselmans, G J Wensink & J Vogelzang, 2001. The Bathymetry Assessment System: efficient depth mapping in shallow seas using radar images. <u>International Journal of Remote Sensing</u>, 22: 2973-2998

15   Melsheimer, C, G Tanck, M Gade & W Alpers, 1999. Imaging of tidal flats by the SIR-C/X-SAR multi-frequency/multi-polarisation synthetic aperture radar. In: Operational Remote Sensing for Sustainable Development, edited by G J A Nieuwenhuis, R A Vaughan & M Molenaar (Balkema, Rotterdam), 189-192

16   Laur, H, P Bally, P Meadows, J Sanchez, B Schaettler, E Lopinto & D Esteban, 2002. ERS SAR Calibration. Derivation of the backscattering coefficient σ^0 in ESA ERS SAR PRI products. Document ES-TN-RS-PM-HL09. (ESA).

17   Erdas, 1999. Erdas Field Guide. (Erdas Inc, Atlanta), 5th edition

18   Herman P M J, 1997. Comparing patterns in macrofauna structure at different scales: within tidal flats, between tidal flats and between estuaries. In: P Thoolen, M Baptist & P Herman. BEON Habitat MICRO-MACRO. BEON report 98-14. (WL Delft Hydraulics & NIOO-CEMO)

19   Fung A K, 1994. Microwave Scattering and Emission Models and Their Applications. (Artech House)

20   Fung A, Z Li & K S Chen, 1992. Backscattering from a randomly rough dielectric surface. IEEE Transactions on Geoscience and Remote Sensing, 30: 356-369

21   Hallikainen M T, F T Ulaby, M C Dobson, M A El-Rayes & L K Wu, 1985. Microwave dielectric behavior of wet soil, Part I: Empirical models and experimental observations. IEEE Transactions on Geoscience and Remote Sensing, 23: 25-34

22   Lewis A J, F M Henderson & D W Holcomb, 1998. Radar fundamentals : the geoscience perspective. In: Principles and Applications of Imaging Radar. Manual of Remote Sensing, volume 2, edited by F M Henderson & A J Lewis (Wiley, New York), 130-181

23   Davidson M W J, T Le Toan, F Mattia, G Satalino, T Maninnen & M Borgeaud, 2000. On the characterisation of agricultural soil roughness for radar remote sensing. IEEE Transcations on Geoscience and Remote Sensing, 38: 630-640